Supporting Information

Plasmon-exciton interactions on single thermo-responsive platforms demonstrated by optical tweezers

By Silvia Hormeño, Neus G. Bastús, Andrea Pietsch, Horst Weller, J.R. Arias-Gonzalez and Beatriz H. Juárez**

Synthesis of Au nanoparticles and CdSe/CdS quantum dots

Synthesis Au nanoparticles

An aqueous (MilliQ water) solution of sodium citrate 2.2 mM (150 mL) was heated in a heating mantle in a 250-mL three-necked round bottom flask for 15 min under vigorous stirring. After boiling started, 1 mL of $HAuCl_4$ (25 mM) was injected. The resulting particles (~10 nm, ~3×10^{12} nanoparticles/mL) are coated with negatively charged citrate ions and hence, well suspended in H_2O.

Conjugation Conditions for Au nanoparticles

The ligands used for the conjugation with Au nanoparticles (NPs) were PEO-NH_2 branched ligands as those used and described in Salcher et al.[1] 100 μL of an amine-terminated PEO aqueous solution (1 mM) was added to 50 mL citrate-stabilized Au NPs and stirred for 30 min at room temperature. Excess of PEO molecules was removed by precipitation (15000 rpm, 10 min) and re-dissolution in MilliQ water. The resultant particles were stable for several months. A similar strategy has been used for the functionalization of Au NPs with peptides and proteins.[2] UV-Vis absorption measurements were acquired to monitor the conjugation. Citrate-stabilized Au NPs displayed a characteristic UV-Vis absorption spectrum with a plasmon band at 522.5 nm (Figure 1B in the main text). The absorption spectrum is sensitive to the NP's environment and a red-shift of about 2 nm can be observed once amine-terminated PEO molecules cover Au NP's surface. The shift occurs in a few seconds suggesting that the conjugation process is quick. The conjugation mechanism is driven by an initial uptake of the molecule via electrostatic interactions (positively charged amino group and negatively charged Au surface).

Synthesis of CdSe/CdS quantum dots and ligand exchange

CdSe/CdS core/shell particles were synthesized according to the work of Mekis et al.[3] A ligand exchange procedure developed by M. Nikolic et al.[4] was applied to make the particles water-compatible by substituting the former ligands by amine-modified poly(ethylene oxide)s (PEOs) ligands. The ligands used for the ligand-exchange procedure are tri-block copolymers like those described in Pöselt et al.[5]

Synthesis of pNIPAM microspheres and NPs immobilization

The synthesis of pNIPAM beads and further immobilization of NPs on their surface was carried out following a method described in previous work,[5] where amino-capped-PEO nanocrystals showed high interaction with pNIPAM beads containing maleic acid (MA) moieties. Briefly, pNIPAM beads were

produced by means of emulsion polymerization with maleic acid and N-N′-methylene-bis-acrylamide as crosslinker.[6] After the synthesis, the beads where thoroughly cleaned by numerous cycles of sonication and centrifugation at 6000 rpm for 20 min. It is essential to obtain a clean bead surface for further incubation with NPs. As previously reported, the incubation of pNIPAM beads containing MA with CdSe@CdS amine-poly(ethylene oxide) ligand exchanged NPs produces highly loaded beads.[1]

In a typical incubation experiment, 0.25 mL of a suspension of pNIPAM beads containing 1.6 mg/mL were first incubated at room temperature for 24 h under stirring with 8 mL of Au NPs (3×10^{12} NP/mL) in a volume of 5 mL. The Au NPs were washed twice by centrifugating at 15000 rpm for 20 min and sonicated in double deionized water prior its incubation. After 24 h, 5 μL of a concentration solution of quantum dots (QDs) 8 μM were added and stirred for 1 h. Centrifugation at 5000-6000 rpm for 20 min and sonication cycles were performed to discard NPs in the supernatant. A quantitative attachment of the QDs is always observed whereas some Au NPs in the supernatant are found. Samples were imaged by Transmission Electron Microscopy to check that homogeneous coverage on the beads surface took place.

Figure S1. Magnified version of Figure 1A. CdSe/CdS (light, small dots) can be distinguished from Au NPs (darker and bigger dots).

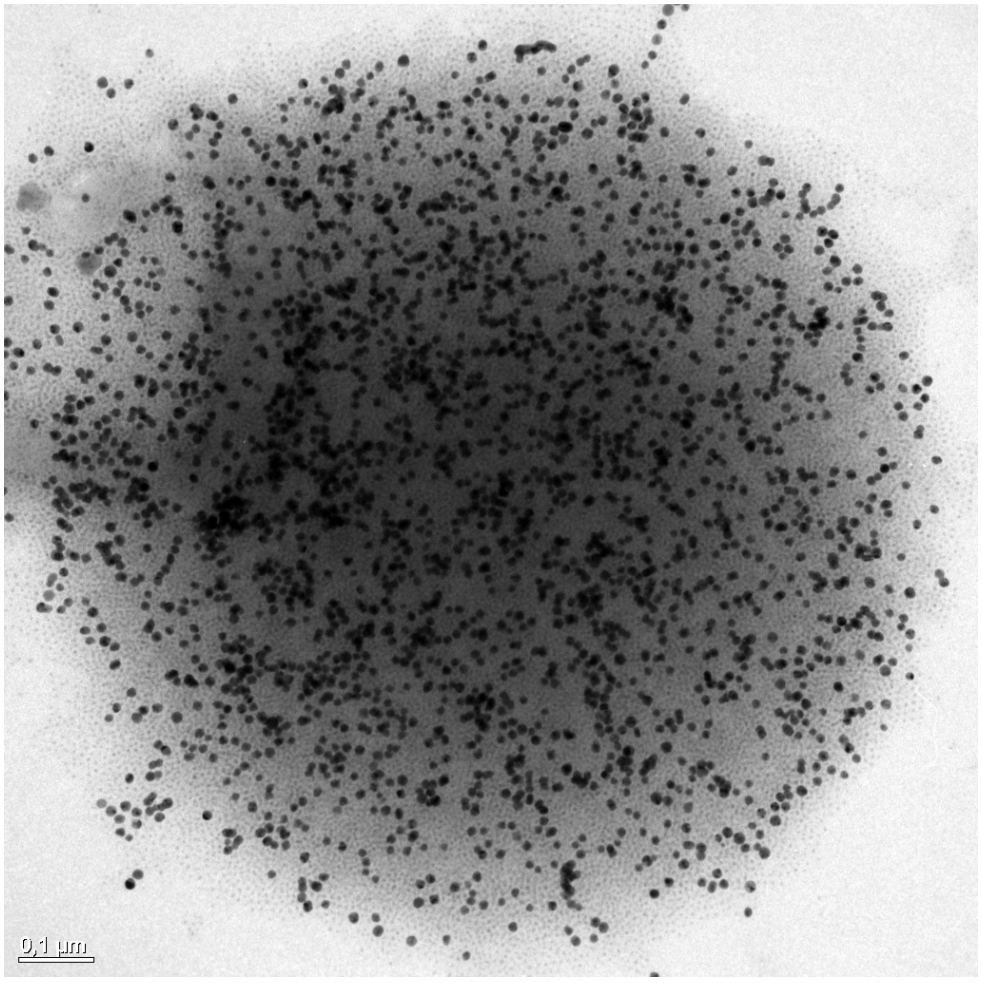

Absorption and emission properties

Absorption measurements were carried out in a Cary 50 spectrophotometer from Varian. Emission properties were measured in a Fluoromax 4 Horiba Yobin Yvon fluorometer. A home-made set-up was used for the temperature dependent photoluminescence measurements.

Experiments with Optical Tweezers

The optical design includes a dual-counterpropagating-beam (λ = 835 nm) optical trap capable of measuring forces as changes in light momentum flux.[7] The force measured by a light-momentum sensor calibrated from first principles (conservation of linear momentum) does not depend on either power or direction of the incident radiation provided that all the scattered light is collected.[7] The two objectives used in this optical tweezers design are Nikon CFI Plan-Apochromat 60X (Nikon Corporation, Tokyo, Japan), water immersion, numerical aperture (NA) 1.2. Each objective is used to both focus and collect light for analysis. Laser light exiting the trap is collected and reflected into position-sensitive photodetectors (PSD) by using quarter-wave plates and polarizing beamsplitter cubes (PBS) as shown in Figure 2A of the main text. The NA of each single beam is around 0.5. We used low-NA beams inside high-NA objectives to allow significant beam deflection while still collecting all the light, thus ensuring force measurement by the calibration based on the conservation of light momentum. To illuminate the trapped object and follow the experiments by videomicroscopy we used a blue LED as a light source and Köhler illumination. The image was monitored by a CCD camera (Watec LCL-903K, Edmund Optics). The blue LED has a power of 80 μW measured in front of the lamp and, as it is strongly attenuated, the power at the exit of the first objective in the laser's optical path falls to ~300 nW. IR and visible filters are placed in front of the CCD camera to process the images for the different assays.

pNIPAM and polystyrene beads used as a control (see main text) were trapped and manipulated with the optical tweezers inside a fluidics chamber. More specifically, they were flowed into the chamber by an automated fluidics system consisting of glass micro-dispensers and polyethylene tubes connected to the sample reservoirs. As described in the main text, a pressure bottle and a glass capillary were used to pump the suspension of pNIPAM particles directly to the central channel of the fluidics chamber (Figure 2A). Two other channels in the fluidics chamber (bottom and top) were used to flow polystyrene particles of different sizes for control experiments. These channels were connected to the central one by glass capillaries (not shown in Figure 2A, see Figure 3 of Hormeno et al.[8]). This design limits the access of different samples to the central channel, where experiments are performed, and allows fast liquid exchanges in this channel for experiments in different conditions. It is also very useful to clean the central channel in the chamber and remove air bubbles which may cause spurious drift in the force measurements. Channels and pressure bottles were connected through expansion bottles, as the one depicted in Figure 2A, to solenoid valves and pressure sensors whose selection was computer-controlled.[9] To allow switching between opposite flow directions in the channels, one valve was connected to a high pressure source, another to a vacuum source (low pressure) and a third one to atmospheric pressure. Flow rates could be established and stopped with high precision so that sorting and selective trapping of individual specimens were quickly accomplished with high throughput. To control trapping of single

specimens, careful observation of diffusive pNIPAM microspheres was accomplished before data collection. Subsequent data analysis was also used to discard spurious assays which may have taken place with multiple microspheres.

Hydrodynamic Size Analysis

We determined the hydrodynamic size by analyzing the thermal noise of optically-trapped pNIPAM microspheres. The equilibrium power spectral density of force fluctuations of an overdamped particle in a harmonic potential can be given by:[10-13] $\langle \Delta F^2(f) \rangle_{eq} = 2\gamma k_B T f_c^2/(f^2+f_c^2)$ in units of force squared per frequency, where ‹..› represents the ensemble average, $f_c = \kappa/2\pi\gamma$ is the so-called corner frequency, γ is the drag coefficient of the particle, k_B is the Boltzmann constant, T is the temperature, κ is the spring constant of the particle in the optical trap and f is the sampling frequency in units of Hertzs. The diameter, d, of the pNIPAM microspheres was derived from the drag coefficient ($\gamma = 3\pi d\eta$, where η is the viscosity of the medium). To that end, a voltage signal proportional to the force exerted by the thermal fluctuations on a trapped pNIPAM microsphere was recorded in intervals of 5.24 s at 100 kHz. The time interval was then split into 128 parts of 40.96 ms. Next, force fluctuations (in voltage units) in each interval were Fourier transformed in the time domain ($-\infty$, $+\infty$) and averaged over the 128 samples. Resulting data, in units of voltage squared per frequency, were fitted to the power spectral density equation shown above to obtain the drag coefficient of the pNIPAM microspheres, γ_{pnipam}. The same procedure was used to obtain the drag coefficient of polystyrene microspheres of known diameter, γ_{bead}, which we used for reference experiments. To set d in common units, we calibrated the size of the pNIPAM microspheres, d_{pnipam}, thus measured, relative to that of the reference beads, d_{bead}, from the ratio of drag coefficients: $d_{pnipam} = d_{bead} \times \gamma_{pnipam} / \gamma_{bead}$.

Hydrodynamic Size Analysis of bare pNIPAM beads in heavy water

To carry out these experiments, a diluted water dispersion of pNIPAM beads was centrifuged at 5000 rpm for 20 min. The supernatant was discarded and the sediment containing the beads was left to partially dry. A new volume of deuterium oxide was added to obtain the new dispersion that was sonicated for 10 min prior to their injection into the chamber. The central channel of the fludics chamber, where the experiments take place, and the glass capillary tube that dispenses the beads into it were filled with D_2O. Hydrodynamic size measurements were performed using the thermal-noise analysis described above. Figure S2 shows the resulting size distribution of pNIPAM beads in D_2O. The histogram was fitted to a Lorentzian distribution and the position of the peak was found at a size of 1123 ± 150 nm (n = 55).

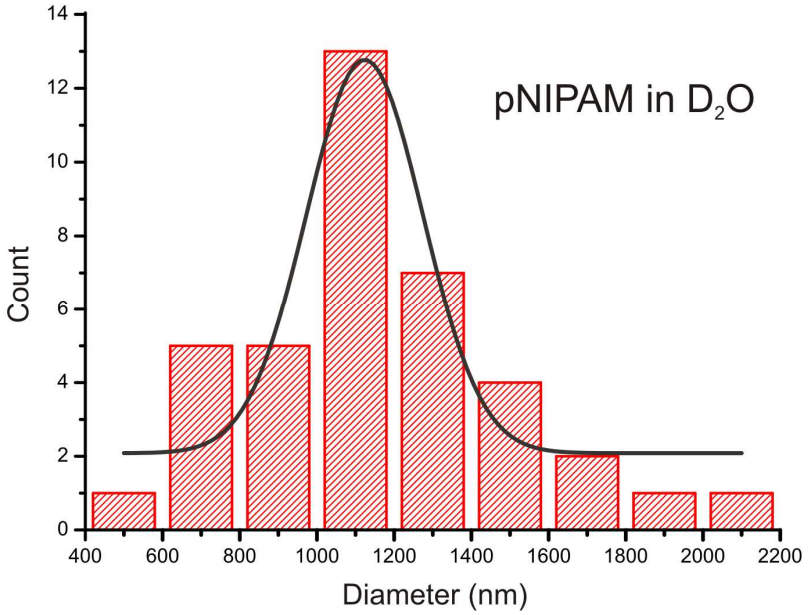

Figure S2. Distribution of hydrodynamic diameters of optically-trapped pNIPAM microspheres in D_2O. Black line is a Lorentzian fit.

Estimation of the heat transferred from Au NPs to pNIPAM beads

Au NPs can efficiently release heat under optical excitation. The electric field of the laser strongly drives mobile carriers inside the Au NPs, and the energy gained by carriers turns into heat. Then, the heat diffuses away from the NP and leads to a temperature increase of the surrounding medium. Heat generation becomes significantly strong for the case of metal NPs in the regime of plasmon resonance.

Under steady state conditions, the radial temperature profile outside the particle can be estimated from the following expression:[14]

$$T(r) = T_{\infty} + \frac{P_{abs}}{4\pi r C} \tag{1}$$

In this equation, T_{∞} is the room temperature, C is the thermal conductivity of water (0.6 W/K·m), r is the distance from the center of the Au NP and P_{abs} is the absorbed optical power by the NP, which is given by $P_{abs}=\sigma_{abs}\cdot I(z)$, being $I(z)$ the laser intensity at position z from the beam focus and σ_{abs} the absorption cross section of a Rayleigh particle,[15]

$$\sigma_{abs} = \frac{2\pi n_w}{\lambda} \mathrm{Im}\left\{3V \frac{\varepsilon_g - \varepsilon_w}{\varepsilon_g + 2\varepsilon_w}\right\}. \tag{2}$$

In this equation, 'Im' denotes imaginary part, λ is the radiation wavelength, n_w is the refractive index of water, ε_w and ε_g are the dielectric permittivities of water and gold, respectively, and V is the volume of the NP.

To provide a gross estimation of the temperature profile, we used two assumptions: (i) the intensity of the beam at the position of the metallic NP is constant and given by $I(z)=P_{laser}/S_{spot}$ (P_{laser}, total laser power at the focal region and S_{spot}, approximate spot area); and (ii) the absorption cross-section of a 10-nm Au NP can be calculated by applying Mie theory for a sphere. The first approximation does not take into account the gradient of the intensity profile in the focal region and therefore the temperature increased by the NPs which are near the center of the beam focus is underestimated and the temperature increased by the NPs which are far away from this position is overestimated. In the second approximation it is assumed that classical electromagnetism is valid for a 10-nm Au particle. A more reliable temperature estimation should be performed by direct measurement of the heating profile around the particle, as performed elsewhere.[16,17]

Figure S3 shows the temperature increase from a single 10-nm Au NP illuminated by two counterpropagating focused beams of λ = 835 nm and $2P_{laser}\approx$140 mW in a focal region of $\approx$ 1 μm^2 ($I \approx 1.8\times10^7$ W/cm^2), as calculated by using eqs. (1) and (2).[18] The absorption cross-section of the NP is 8.7×10^{-15} cm^2, as calculated by using MiePlot software with corrections for particles beyond the Rayleigh limit. The power absorbed by the NP is $P_{abs} \approx 1.6\times10^{-7}$ W. This calculation does not take into account the diffusion of water molecules surrounding the pNIPAM platform, which may vary during the heating process.

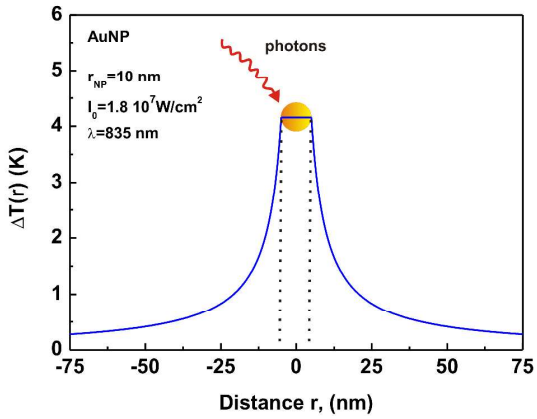

Figure S3. Temperature-increase profile around a 10-nm Au sphere

The heating dynamics for an Au NP surrounded by water is relatively fast and can be estimated from[18]

$$t = r_{NP}^2\left(c\rho / k\right), \qquad (3)$$

where ρ, c, k are the mass density, specific heat capacity and thermal conductivity of water. For a 10-nm Au NP, a heating time of ~7 ns is obtained by using eq. (3). This number should be taken with care since it does not account for the heating dynamics of a spherical-shell distribution of Au NPs (see main text).

Supplementary videos

Video S1. Photoluminescence of a single pNIPAM/QDs microsphere in the optical trap. The microsphere describes a random walk before falling into the optical trap (the position of the microsphere is marked by a flashing arrow to help following its trajectory). When the illumination lamp is turned off, the fluorescence intensity of QDs is observed.

Video S2. Photoluminescence of a single pNIPAM/Au/QDs microsphere in the optical trap. When the microsphere is trapped, the illumination lamp is turned off and the emission and quenching of QDs becomes observable. As shown by the timer (h:m:s:ms) in the bottom-left corner, the frame rate has been increased by 2.6X.

Supporting References

1. Salcher, A.; Nikolic, M. S.; Casado, S.; Velez, M.; Weller, H.; Juarez, B. H. *Journal of Materials Chemistry* **2010**, 20, (7), 1367-1374.
2. Bastús, N. G.; Sanchez-Tillo, E.; Pujals, S.; Farrera, C.; López, C.; Giralt, E.; Celada, A.; Lloberas, J.; Puntes, V. *ACS Nano* **2009,** 3, (6), 1335-44.
3. Mekis, I.; Talapin, D. V.; Kornowski, A.; Haase, M.; Weller, H. *Journal of Physical Chemistry B* **2003,** 107, (30), 7454-7462.
4. Nikolic, M. S.; Krack, M.; Aleksandrovic, V.; Kornowski, A.; Forster, S.; Weller, H. *Angew. Chem.-Int. Edit.* **2006,** 45, (39), 6577-6580.
5. Pöselt, E.; Fischer, S.; Foerster, S.; Weller, H. *Langmuir* **2009**, 25, (24), 13906–13913.
6. Das, M.; Sanson, N.; Fava, D.; Kumacheva, E. *Langmuir* **2007,** 23, (1), 196-201.
7. Smith, S. B.; Cui, Y.; Bustamante, C. *Methods Enzymol* **2003,** 361, 134-62.
8. Hormeno, S.; Arias-Gonzalez, J. R. *Biol Cell* **2006,** 98, (12), 679-95.
9. Wuite, G. J.; Davenport, R. J.; Rappaport, A.; Bustamante, C. *Biophys J* **2000**, 79, (2), 1155-67.
10. Wang, M. C.; Uhlenbeck, G. E. *Rev. Mod. Phys. J1 - RMP* **1945,** 17, (2-3), 323 LP - 342.
11. Berg-Sorensen, K.; Flyvbjerg, H. *Review of Scientific Instruments* **2004,** 75, (3), 594-612.
12. Mao, H.; Arias-Gonzalez, J. R.; Smith, S. B.; Tinoco, I., Jr.; Bustamante, C. *Biophys J* **2005,** 89, (2), 1308-16.
13. Hormeno, S.; Ibarra, B.; Chichon, F. J.; Habermann, K.; Lange, B. M.; Valpuesta, J. M.; Carrascosa, J. L.; Arias-Gonzalez, J. R. *Biophys J* **2009,** 97, (4), 1022-30.
14. Andrä, W.; d'Ambly, C. G.; Hergt, R.; Hilger, I.; Kaiser, W. A. *J. Magn. Magn. Mater.* 194 (1999) 197-203.
15. van de Hulst, H. C. *Light scattering by small particles*. Dover, New York (1981)
16. Bendix, P.; Nader, S.; Oddershede, L.B.; *ACS Nano* **2010**, 4, (4), 2256-2262.
17. Kyrsting, A.; Bendix, P.; Stamou, G.; Oddershede. L.B. *Nano Letters* **2011**,11, (2), 888-892.
18. Govorov, A. O.; Zhang, W.; Skeini, T.; Richardson, H.; Lee, J.; Kotov, N. A. *Nanoscale Research Letters* **2006,** 1, (1), 84-90.